Journal of Laser Applications

Application of adjustable ring mode laser in remote laser welding of additive manufactured AlSi10Mg alloy

Cite as: J. Laser Appl. **34**, 042007 (2022); https://doi.org/10.2351/7.0000794
Submitted: 27 June 2022 • Accepted: 23 August 2022 • Published Online: 20 September 2022

Tianzhu Sun, Nesta Ferguson, Conghui Liu, et al.

Journal of Laser Applications ARTICLE scitation.org/journal/jla

Application of adjustable ring mode laser in remote laser welding of additive manufactured AlSi10Mg alloy

Cite as: J. Laser Appl. 34, 042007 (2022); doi: 10.2351/7.0000794
Submitted: 27 June 2022 · Accepted: 23 August 2022 ·
Published Online: 20 September 2022

Tianzhu Sun,[1,a)] Nesta Ferguson,[2] Conghui Liu,[3] Greg Gibbons,[1] and Pasquale Franciosa[1]

AFFILIATIONS

[1]WMG, University of Warwick, Coventry CV4 7AL, United Kingdom
[2]School of Engineering, University of Warwick, Coventry CV4 7AL, United Kingdom
[3]School of Materials, The University of Manchester, Manchester M13 9PL, United Kingdom

Note: Paper published as part of the special topic on Proceedings of the International Congress of Applications of Lasers & Electro-Optics 2022.

[a)]**Author to whom correspondence should be addressed; electronic mail:** Tianzhu.Sun@warwick.ac.uk

ABSTRACT

Additive manufacturing (AM) is an innovative manufacturing technology that offers the ability to build parts with both geometric and material complexities. However, limitations, including low build volume capability and production rate, yield its rapid application in high volume production. This paper presents the potential of remote laser welding (RLW) as a post-AM joining approach to scale up the AM components. The AM AlSi10Mg alloy was fabricated by direct metal laser sintering and subsequently joined by RLW without filler wire or shielding gas. A novel adjustable ring mode (ARM) laser beam was employed during the RLW process where the ring beam is designed to stabilize the keyhole by providing the preheating and postheating while the core beam guarantees a sufficient weld penetration. The impact of the ARM laser on weld porosity was evaluated in both fillet lap and bead-on-plate welding configurations, accompanied by the variation of core/ring beam power ratios. Crack-free welds with promising weld appearance were obtained among all welding trials, indicating that the ARM-RLW process can be employed for the robust connection of AM AlSi10Mg alloys. Optimizing the power ratio can substantially reduce the weld porosity area ratio from 24.3% to 13.5% in the fillet lap configuration and from 24.2% to 14.4% in the bead-on-plate configuration. Analysis of variance tests statistically confirmed the significant impact of the power ratio on the porosity area ratio. Future work has been suggested for the process maturation of RLW as a post-AM joining approach in industrial application.

Key words: remote laser welding, adjustable ring mode laser, porosity, power ratio, additive manufactured AlSi10Mg

I. INTRODUCTION

Geometrical complexity is one of the core challenges in producing industrial components by traditional subtractive manufacturing processes. Taking advantage of the layer-by-layer manufacturing strategy, additive manufacturing (AM) brings the chance to produce near-net-shape workpieces, leading to a substantial reduction in lead time, material waste, and carbon footprint.[1] A direct cost saving of up to 69% has been reported for producing a 2.5 mm thick truncated cone through AM instead of the conventional method consisting of forging and postmachining.[2] AlSi10Mg is an industry-attractive alloy characterized by a high strength-to-weight ratio, sound castability, and excellent corrosion resistance.[3] Recent advancements in metal AM technology have achieved ~99% relative density[3] and nearly identical electric resistivity[4] of AM AlSi10Mg compared to its cast counterpart. These lead to promising applicability of AM AlSi10Mg alloys in the E-mobility, for example, AM gussets as part of battery casings[5] and AM electrical windings within electric motors.[4]

However, significant challenges must be addressed before AM can be adopted as a viable high-volume production process.

Difficulty in controlling fusion pores and residual stresses during the manufacture of large components, coupled with the low build volume capability and production rate, limits the scalability of the current technology.[6] In this regard, welding as the post-AM processing technique for joining the printed AM components bridges the gap between the current situation and increasing demands of AM products while providing a production scalable and economical solution. There have been several feasibility investigations on the welding of AM AlSi10Mg alloys. For example, Nahmany *et al.*[7,8] demonstrated the electron beam welding of AM AlSi10Mg alloys and determined a joint strength close to the base material. Scherillo *et al.*[9] investigated friction stir welding of AM AlSi10Mg components and reported an improved hardness within the welded region compared to the base material attributing to the grain refinement. In addition, researchers have attempted laser welding as an alternative approach due to the high processing speed, noncontact characteristics, and precise control of the beam position, which offer process flexibility, especially when joining AM parts with complex geometry. Zhang *et al.*[10] compared TIG welding and laser beam welding of AM AlSi10Mg and observed a significantly improved weld appearance of laser welded joints. The authors also reported that the high porosity susceptivity is the dominant challenge of AM AlSi10Mg alloys subjected to laser welding. The frequent formation of pores is associated with two phenomena: (1) growth and coalescence of the pre-existed microvoids in the AM components and (2) precipitation of the dissolved hydrogen originating from the oxide films covering powder.

Minimizing the hydrogen content of AM alloy is one solution to reducing porosity in laser welded AM joints, for example, drying the power and optimizing the AM processing parameters,[11] which are beyond the scope of this study. Recently, researchers have also focused on the optimization of the laser welding process. Chen *et al.*[12] reported that the high-pressure ambiance during laser welding could significantly reduce weld porosity since the growth and merging of micropores were significantly limited. It should be noted that the mitigation of weld porosity, in this case, comes at the cost of weld penetration. Emmelmann and Beckmann[13] demonstrated that the multimode laser is beneficial for porosity reduction as compared to the single-mode laser. The authors further reported that an increasing welding speed and a narrower beam oscillation path can substantially reduce the pore size due to a more rapid solidification process.

The adjustable ring mode (ARM) laser beam, introduced by Coherent Inc,[14] is a novel beam shaping technique, consisting of an inner core beam and outer ring beam, and offers the flexibility of in-process modification of thermal profile. The core beam, having a higher energy intensity, guarantees sufficient weld penetration. The leading edge of the ring beam provides the preheating, resulting in the increasing energy absorption rate, and the trailing edge of the ring beam supplies the postheating, enlarging the molten pool and promoting the escape of gas bubbles. Several studies have demonstrated improved surface quality and keyhole stability by the employment of the ARM technique.[15–17] Additionally, Sokolov *et al.*[18] determined apparent mitigation of weld porosity during the ARM welding of die-casting aluminum alloys.

Motivated by the promising performance in ARM laser welding of conventionally manufactured alloys, this study aims to investigate the impact of the ARM laser on the porosity formation in laser-welded AM AlSi10Mg joints. The ARM laser was integrated into the remote laser welding system, which is widely adopted in the automotive industry nowadays because of its high productivity and flexibility. Case studies in the fillet lap and bead-on-plate joint configurations were present, accompanied by different core/ring power ratios.

TABLE I. Nominal chemical composition of AM ALSI20MG alloy (wt. %).

Si 9%–11%	Fe 0.55%	Mn 0.45%	Mg 0.2%–0.4%
Ti 0.15%	O 0.1%	Zn 0.1%	Al Bal.
<0.05% (Cu, Pb, Ni, N, Sn)			

II. EXPERIMENTAL PROCEDURE

A. Specimen design and preparation

AlSi10Mg plates having a geometry of $40 \times 70 \times 2.5\ mm^3$ for the fillet lap welding configuration and $40 \times 70 \times 3.5\ mm^3$ for the bead-on-plate welding configuration were produced by the direct metal laser sintering AM technique on the EOSM280 system. The nominal chemical composition of the AlSi10Mg alloy is shown in Table I. After the AM process, plates were first heat-treated at 250 °C for 2 h to release residual stresses and then cleaned with compressive air to remove the residual AlSi10Mg powder.

B. Welding setup and process parameters

A 10 kW ARM fiber laser source (HighLight FL10000-ARM, Coherent) was employed and delivered by the Precitec WeldMaster remote welding head. Specifications of the welding system are listed in Table II.

Experimental setups of fillet lap and bead-on-plate joint configurations are schematically illustrated in Fig. 1. The welding direction is consistent with the build direction of the AM process. Transverse beam oscillation was used in the fillet lap welding tests for the purpose of good weld shape,[19,20] leading to a Sine wave laser path at a frequency of 200 Hz and an oscillation width of 2 mm. The center of the oscillation path was set to be 0.2 mm away from the edge of the upper part in the *y*-direction. A linear laser path was employed in the bead-on-plate welding trials. Table III lists the detailed process parameters. For the case study of fillet lap welding, welds were produced with a fixed core beam power and gradually increasing ring power, which were replicated at different

TABLE II. Technical specifications of the welding system employed in this study.

FL-ARM 10 000 and WeldMaster	Core	Ring
Maximum output power (W)	5000	5000
Optical fiber diameter (μm)	100	290
Spot diameter at the focus (μm)	200	580
Emission wavelength (nm)	1080	
Rayleigh length (mm)	5.3	
Focusing length (mm)	300	
Collimating length (mm)	150	

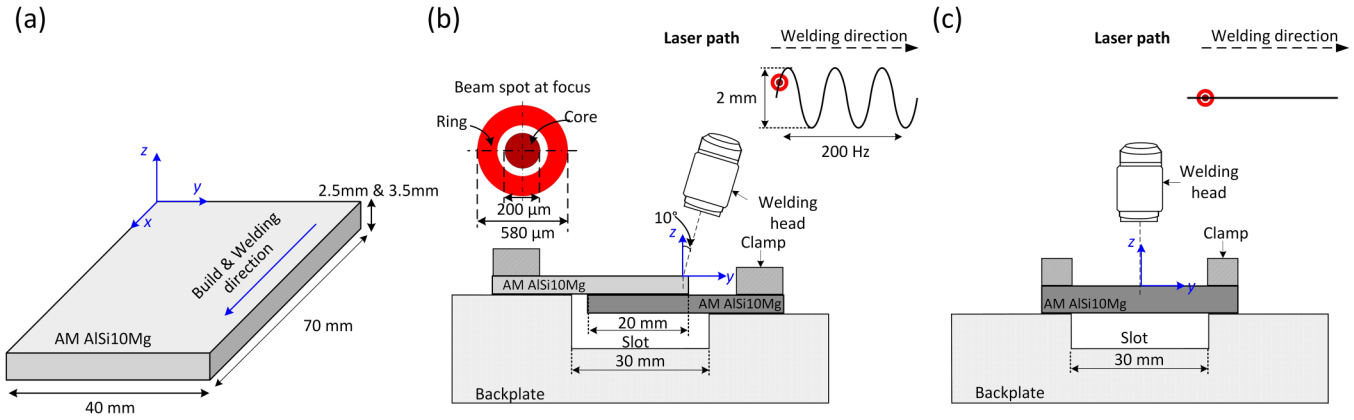

FIG. 1. Schematic diagram showing (a) geometry of AM plate and welding direction in relation to the AM building direction, and experimental set-up of laser welding in (b) the fillet lap configuration and (c) the bead-on-plate configuration.

vertical focal offsets. The focal offset of 0 mm refers to the upper part's top surface, and the negative values correspond to defocusing inside the material. For the case study of bead-on-plate welding, trials were conducted with a fixed total power and different core/ring power ratios, replicated at two welding speeds, while remaining the same linear energy. All experiments were performed without shielding gas or filler wire.

C. Weld characterization

After welding, three transverse (y–z) cross sections were produced for each weld plate and processed following the standard metallographic preparation, consisting of grinding with silicon carbide paper (P1200, P2500, and P4000) and polishing with diamond suspensions (3 and 1 μm) and colloidal silica suspensions (0.06 μm). Optical images of each cross section were obtained on a Keyence VHX7000 optical microscope and processed in IMAGEJ for the weld porosity analysis. The porosity area ratio (total porosity area divided by the fusion zone area) is used to evaluate porosity levels.

Weld zone grain structure was characterized by EBSD mapping on the transverse cross section. Experiments were conducted on a JEOL 7800F scanning electron microscope, equipped with an Oxford Instruments' Symmetry II EBSD detector and AZtec acquisition software with an accelerating voltage of 20 kV and a step size of 3 μm.

III. RESULTS AND DISCUSSION

A. Case study 1: Fillet lap configuration

Figure 2 shows cross sections of fillet lap welds produced with increasing ring powers in the column (at fixed core power) and various vertical focal offsets in the row. The fusion boundary of each weld was expressed by the red dashed line. All welds are free from

TABLE III. Definition of process parameters employed in this study.

Case study 1: Fillet lap configuration (fixed core beam power)			
Welding speed (mm/s)	67	Oscillation width (mm)	2
Oscillation frequency (Hz)	200	Vertical focal offset (mm)	−4; −2; 0; +2; +4
Core power (W)	3125	Ring power (W)	2230; 2680; 3350; 4465
Core/ring power ratio	1.40; 1.17; 0.93; 0.70	Total power (W)	5355; 5805; 6475; 7590
Linear energy (J/mm)	80; 87; 97; 114		
Case study 2: Bead-on-plate configuration (fixed total power)			
Welding speed (mm/s)	67; 100	Vertical focal offset (mm)	0
Core power at a welding speed of 67 mm/s (W)	810; 1080; 1355; 1625; 1910; 3250	Ring power at a welding speed of 67 mm/s (W)	2440; 2165; 1900; 1625; 1340; 0
Core power at a welding speed of 100 mm/s (W)	1230; 1640; 2050; 2460; 2895; 4920	Ring power at a welding speed of 100 mm/s (W)	3690; 3280; 2870; 2460; 2030; 0
Core/ring power ratio	0.33; 0.50; 0.70; 1; 1.43; Core only		
Total power (W)	3250; 4920	Linear energy (J/mm)	49

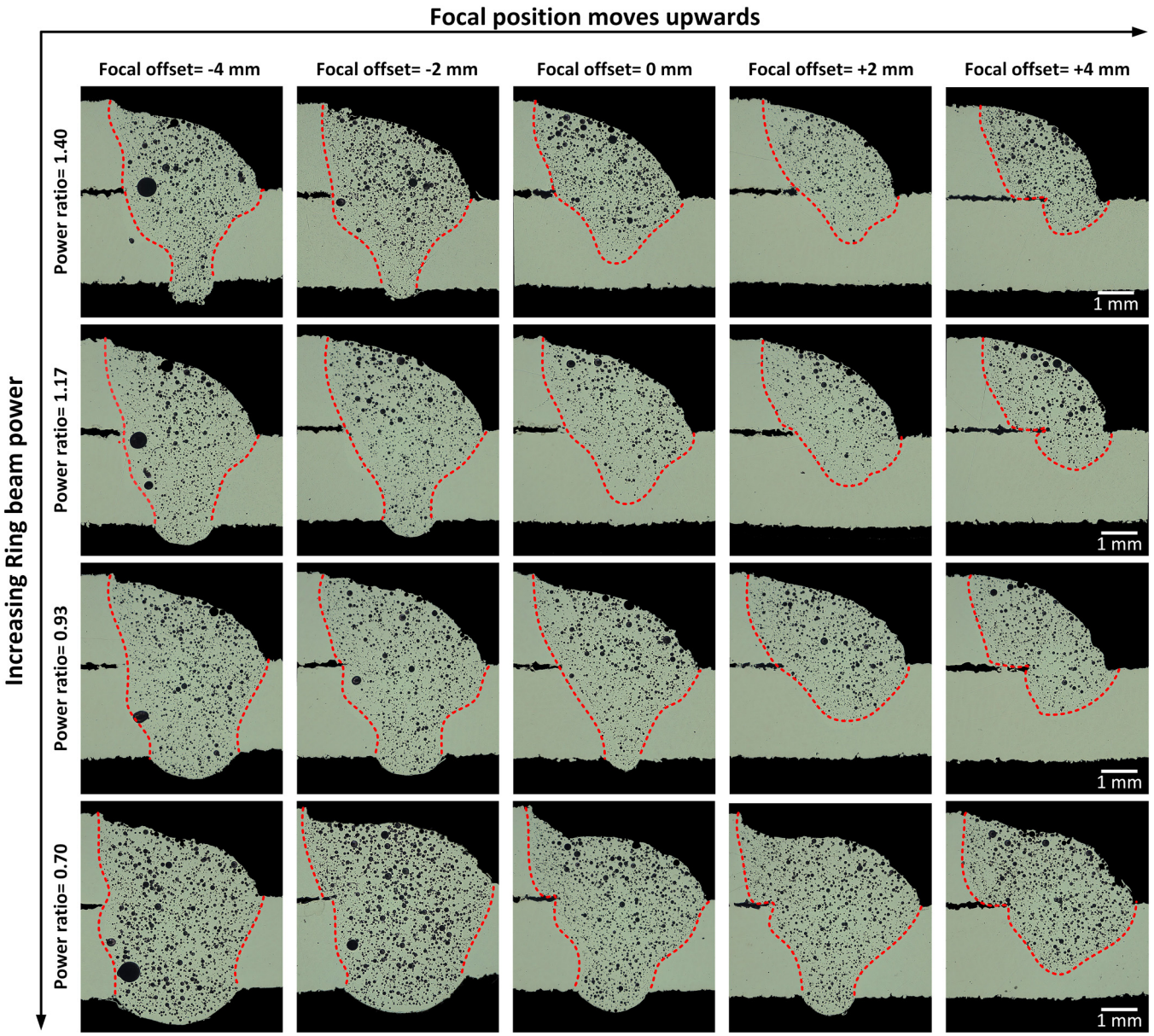

FIG. 2. Cross-section images of welds produced in the fillet lap configuration. Note that the fusion boundary is expressed by the red dashed line.

hot cracking, and no apparent surface defect was determined. It can be seen that increasing the ring power and defocusing inside the material can lead to the growth of weld penetration and width of the fusion zone at the interface of two plates due to the increase in power density. In addition, spherical-shaped pores were determined in all welds regardless of the change in power ratios and focal offsets, and they are uniformly distributed in the fusion zone. The evolutions of porosity area ratio as a function of power ratios and focal offsets are shown in Fig. 3. A V-shape distribution is determined between porosity area ratio and power ratio, with the minimum porosity level at a medium power ratio (1.17 or 0.93). In addition, this finding is applicable to all focal offset levels. A two-way analysis of variance (ANOVA) with the confidence value of 0.05 was conducted to demonstrate the effects of power ratio and focal offset on the weld porosity. A p-value of 0.0016 for the test between power ratio and porosity area ratio and a p-value of 0.1150 for the test between focal offset and porosity area ratio were determined. These results statistically confirm that only the power ratio significantly impacts the weld porosity area ratio.

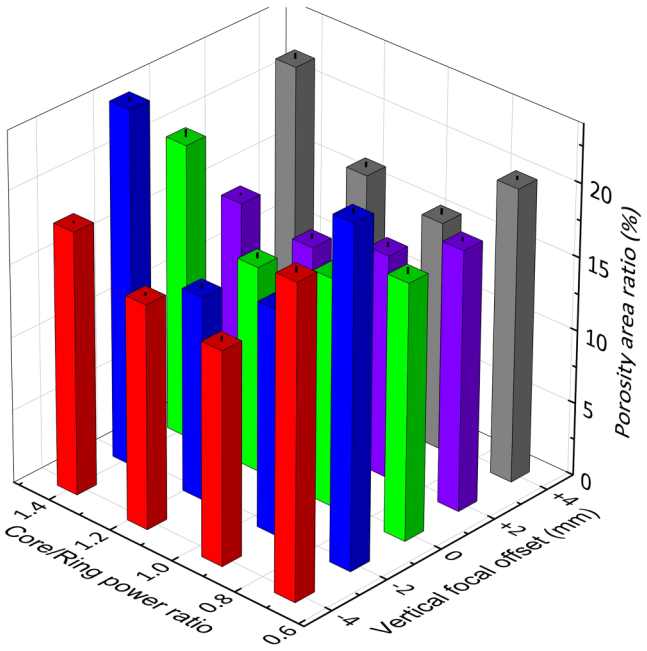

FIG. 3. Porosity area ratios of fillet lap welds with various core/ring power ratios and vertical focal offsets. Note that the core beam is fixed and the power ratio is altered by increasing the power ring beam.

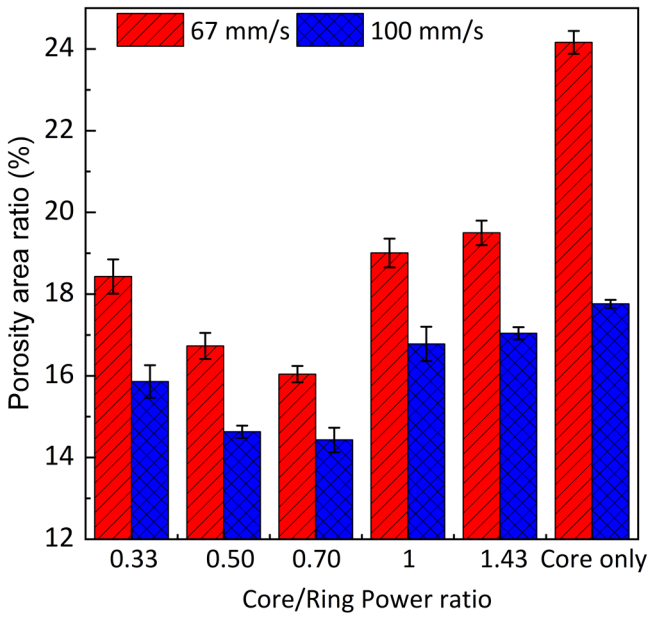

FIG. 5. Porosity area ratios of bead-on-plate welds with various core/ring power ratios and welding speeds. Note that constant total powers of 3250 and 4920 W were used for welding at 67 and 100 mm/s, respectively, leading to the identical linear energy among all welds.

B. Case study 2: Bead-on-plate configuration

Figure 4 shows cross sections of bead-on-plate welds produced with various core/ring power ratios in the row (at fixed total power) and different welding speeds in the column. Although reducing the power ratio leads to lower beam intensity, sufficient weld penetration is obtained in all welding trials. In addition, due to the excessive beam intensity, top surface undercut and overpenetration were determined when using the single-mode laser (the case of core only weld). Similar to the case of fillet lap welds, a large number of pores were uniformly distributed in the bead-on-plate welds. Figure 5 provides the quantitative summary of porosity area ratios in different welds. For both welding speeds, weld porosity is first inhibited with an increasing power ratio and then promoted as

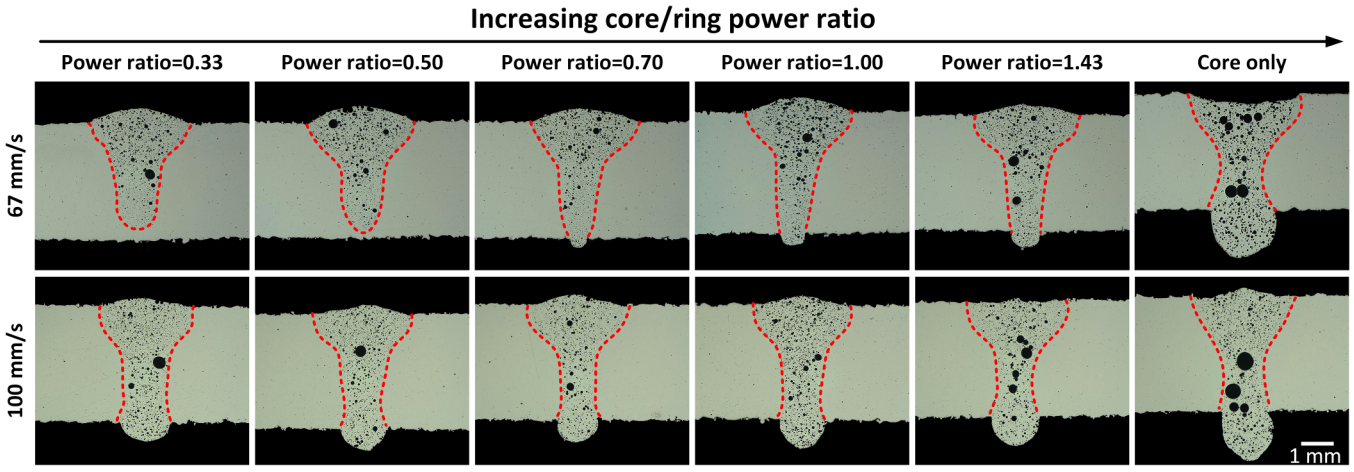

FIG. 4. Cross-section images of welds produced in the bead-on-plate configuration. Note that the fusion boundary is expressed by the red dashed line.

the power ratio further increases, leading to the minimum porosity at the medium power ratio of 0.70. In addition, the porosity area ratio is significantly reduced when a higher welding speed is employed. This is because the reduced laser-material interaction time at a higher welding speed results in a shorter period for the growth and coalescence of tiny pores in the molten pool. A two-way ANOVA with the confidence value of 0.05 was conducted to demonstrate the effect of power ratio and welding speed on the weld porosity in the bead-on-plate configuration. A p-value of 0.0011 for the test between power ratio and porosity area ratio and a p-value of 0.0002 for the test between welding speed and porosity area ratio were determined, statistically confirming that both power ratio and welding speed have significant effects on the weld porosity.

C. Porosity formation mechanism

As discussed in recent studies,[10,19] the high porosity susceptivity of AM AlSi10Mg alloys subjected to laser welding is mainly due to the presence of tiny bubbles developed during the AM and the welding process as a result of the precipitation of dissolved hydrogen. Once formed, these tiny bubbles merge and coalesce as they move following the material flow within the molten pool. Therefore, the time duration of molten pool material remaining in the liquid phase is one of the critical factors determining the extent of the growth and coalescence of tiny bubbles and, consequently, the porosity area ratio.

Representative grain structure maps of fillet lap welds and bead-on-plate welds are obtained by EBSD and shown in Fig. 6. For the fillet lap welds [Fig. 6(a)], columnar grains nucleate near the grain boundary and grow toward the weld center (located in the top right of the weld seam). The solidification direction expressed by the orientation of columnar grains indicates a gradual reduction of the time duration of temperature above solidus from the fusion boundary to the weld center. This explains the presence of tiny pores near the fusion boundary and relatively large pores near the weld center as seen in Fig. 2. The impact of power ratio on the weld porosity is schematically illustrated in Fig. 7(a). For the case of a high power ratio (corresponding to a low total power), a shallower fusion zone and lower molten pool temperature are expected compared to the medium power ratio, which in principle is beneficial for the reduction of weld porosity due to a shorter time for the development of pores. However, a higher porosity area ratio is observed at the high power ratio across all welding groups with different focal offsets. This could be attributed to the reduced postheating provided by the trailing edge of the ring beam, which leads to a more rapid cooling near the seam center and less chance for the escape of bubbles from the molten pool. Therefore, a greater amount of pores were observed near the weld top surface. For the case of a low power ratio (corresponding to a high total power), overall, a high molten pool temperature is expected, leading to a longer time for the development of weld porosity. In addition, since a transition from partial penetration to full penetration occurs, the bottom surface of the molten pool is exposed to the air rather than being surrounded by the solid material having high thermal conductivity (as seen in the case of partial penetration). This leads to a delayed cooling process and a longer time for the development of pores at the weld bottom. Meanwhile, the formation of bugles on the bottom surface indicates that the sum of hydrostatic pressure and hydrodynamic pressure exceeds the surface tension,[21] causing the localized downward material flow, which delays the rise of bubbles for escape from the weld top surface. Therefore, more bubbles were observed at both the weld bottom and top region compared to the case with a medium power ratio.

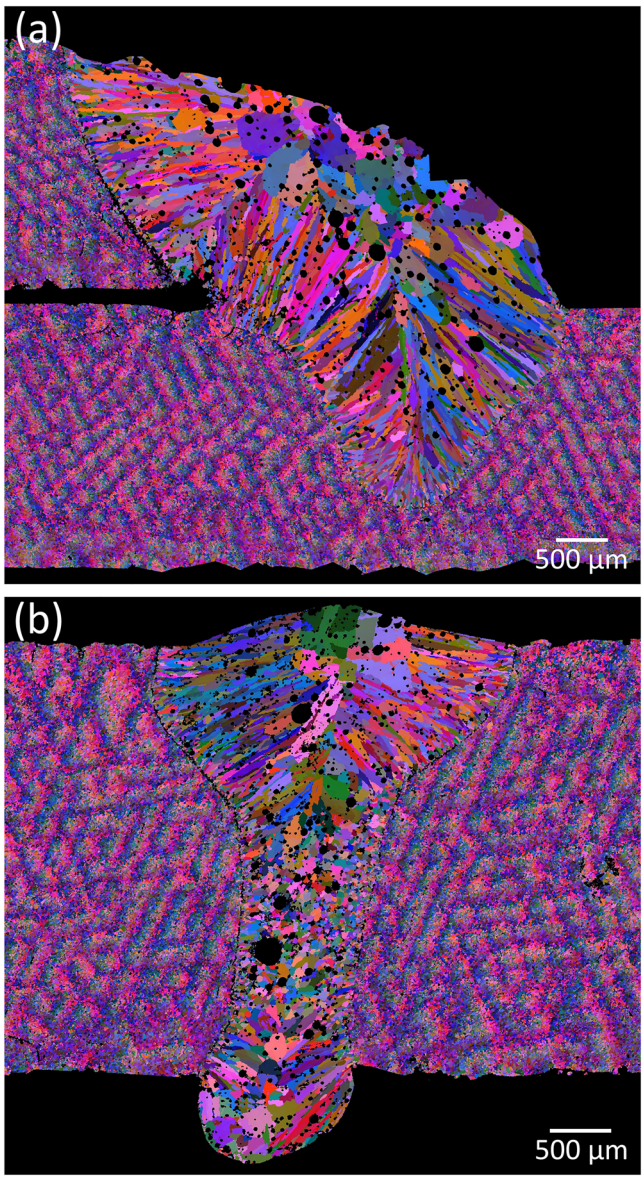

FIG. 6. EBSD Euler maps showing the representative grain structure of AM AlSi10Mg laser welds in (a) the fillet lap configuration and (b) the bead-on-plate configuration. Note that map in (a) refers to the weld produced at the power ratio of 1.17 and a focal offset of 0 mm, and map in (b) refers to the weld produced at the power ratio of 0.70 and a welding speed of 100 mm/s.

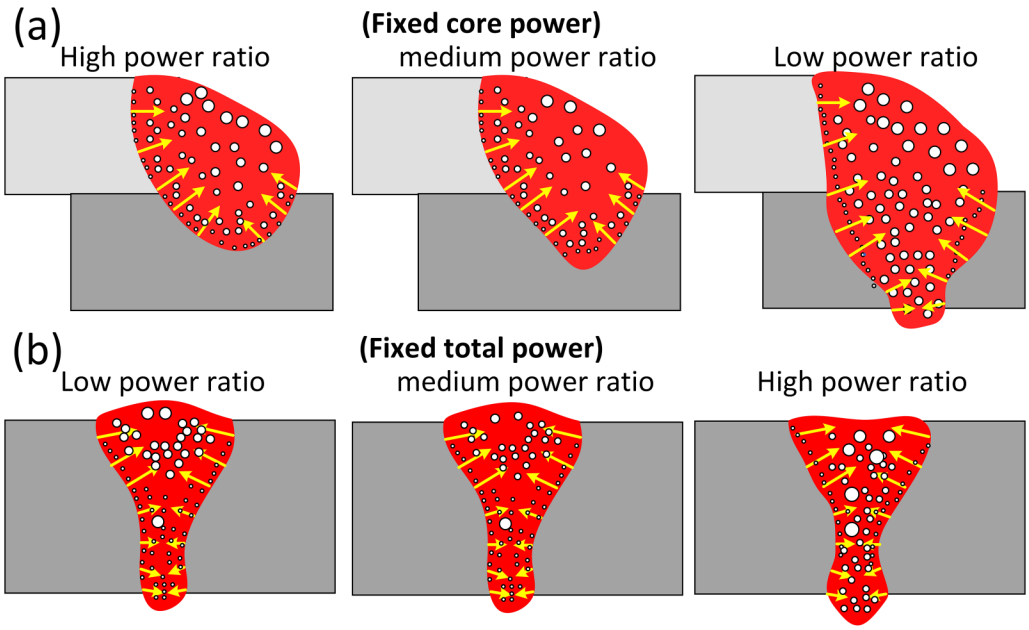

FIG. 7. Schematic diagram showing the evolution of weld porosity of welds with different power ratios: (a) case study of the fillet lap welds (fixed core power) and (b) case study of bead-on-plate weds (fixed total power). The yellow arrows schematically illustrate the solidification direction.

For the bead-on-plate welds [Fig. 6(b)], columnar grains are observed near the weld top and bottom surfaces, both growing from the middle part of the weld. This indicates that the temperature at the weld top and bottom is higher than that at the middle part of the weld, which is consistent with the simulation work reported in Ref. 21. The impact of power ratio on the weld porosity is schematically illustrated in Fig. 7(b). For the case of a low power ratio, more power is assigned to the ring beam, leading to a beam profile with reduced intensity but a wider waist. Consequently, the longer laser-material interaction time and delayed cooling provide a longer time for the development of weld porosity near the weld surface. For the high power ratio, taking the extreme condition of the pure core beam as an example, more energy is absorbed by the material due to the high beam intensity and hence deeper keyhole, leading to overpenetration and higher molten pool temperature. Therefore, a higher porosity susceptivity is expected. It is also interesting to see that when a high power ratio is employed, extremely large pores are more frequent near the weld's middle thickness, where the fusion zone is significantly narrower. This could be attributed to the keyhole collapse as the keyhole tends to be less stable in the weld with excessive penetration.[21] Future work will be conducted on the introduction of the wobbling technique, which provides a more stable material flow,[22] despite the complex impact of oscillation amplitude and frequency on the porosity susceptivity of AM components.[13]

IV. CONCLUSIONS AND FINAL REMARKS

This paper investigated the impact of an ARM laser beam on the weld porosity of AM AlSi10Mg alloys during remote laser welding. Case studies in fillet lap and bead-on-plate welding configurations were presented, accompanied by the variation of core/ring beam power ratios in the fixed core beam power approach and fixed total power approach, respectively. The main findings are summarized below:

- Crack-free AM AlSi10Mg welds can be successfully produced by remote laser welding using an ARM laser beam. ARM laser provides flexibility in optimizing weld geometry by designing the core/ring power ratio.
- Weld porosity is the main challenge of laser welded AM AlSi10Mg joints in both fillet lap and bead-on-plate configurations. As confirmed by ANOVA tests, the ARM laser power ratio and welding speed significantly impact the porosity area ratio.
- A reduction of weld porosity area ratio from 24.3% to 13.5% in the fillet lap configuration and from 24.2% to 14.4% in the bead-on-plate configuration was determined. In both welding configurations, the minimum weld porosity was determined in welds with a medium power ratio (~1 for the fillet lap joint and 0.7 for the bead-on-plate joint).

Even though ARM laser demonstrates a distinct impact on the control of weld porosity, it is not sufficient to reach a porosity-free weld. Future work for the process maturation of RLW as a post-AM joining approach in industrial application is listed below:

- Both case studies in this paper demonstrate that the minimum weld porosity area ratio is associated with the weld at a medium

power ratio, although they differ in welding configuration and the approach to adjusting the power ratio. This motivates further study on the impact of power ratio on the thermal history and material flow behavior through multiphysical simulation work.

- Since AlSi10Mg powder is the primary source of oxygen and hydrogen that eventually leads to the formation of pores, it is worth evaluating the impact of laser cleaning, an efficient approach to remove the residual powder and oxide layers, on the control of weld porosity. This also provides the potential of integrating postcleaning and postjoining techniques into the current AM process due to the similarity in energy delivery methods.

- Ultrasound-assisted laser welding has been investigated in the joining of conventionally manufactured alloys, which significantly impacts pore outgassing and microstructure refinement. It is, therefore, necessary to evaluate its effectiveness in joining AM alloys. Obviously, the feasibility of the joint with a complex geometry is the core factor determining its application in mass production as a solid contact is generally required for the ultrasound technique.

- Considering the compatibility with ARM laser and avoiding compromise to processing efficiency, it is crucial to investigate the impact of the wobbling technique on the control of weld porosity, for example, circular, "8" and infinite oscillation modes.

- Feasibility of welding at a higher welding speed—currently, the maximum tested speed is 100 mm/s—with the aim to shorten the time for growth and coalescence of small pores and also increase production efficiency.

ACKNOWLEDGMENTS

This work was partially supported by WMG Centre High Value Manufacturing Catapult and Innovate UK FASA: Flexible, Automated Stator Assembly. The authors would like to acknowledge the support by the WMG Characterization Facility, partially funded by Higher Education Funding Council for England (HEFCE) and the WMG Centre High Value Manufacturing Catapult. T. Sun would also like to thank Philip Gibbons for helping with the additive manufacturing of AlSi10Mg alloys.

AUTHOR DECLARATIONS

Conflict of Interest

The authors have no conflicts to disclose.

Author Contributions

Tianzhu Sun: Conceptualization (equal); Data curation (equal); Formal analysis (equal); Investigation (equal); Methodology (equal); Visualization (equal); Writing – original draft (equal); Writing – review & editing (equal). **Nesta Ferguson:** Data curation (equal); Formal analysis (equal). **Conghui Liu:** Data curation (equal); Formal analysis (equal). **Greg Gibbons:** Investigation (supporting); Resources (equal). **Pasquale Franciosa:** Funding acquisition (equal); Project administration (equal); Supervision (equal); Writing – review & editing (equal).

REFERENCES

[1]W. E. Frazier, "Metal additive manufacturing: A review," J. Mater. Eng. Perform. **23**, 1917–1928 (2014).
[2]M. K. Thompson, G. Moroni, T. Vaneker, G. Fadel, R. I. Campbell, I. Gibson, A. Bernard, J. Schulz, P. Graf, B. Ahuja, and F. Martina, "Design for additive manufacturing: Trends, opportunities, considerations, and constraints," CIRP Ann. Manuf. Technol. **65**, 737–760 (2016).
[3]K. Kempen, L. Thijs, J. Van Humbeeck, and J. P. Kruth, "Mechanical properties of AlSi10Mg produced by selective laser melting," Phys. Procedia **39**, 439–446 (2012).
[4]C. Silbernagel, I. Ashcroft, P. Dickens, and M. Galea, "Electrical resistivity of additively manufactured AlSi10Mg for use in electric motors," Addit. Manuf. **21**, 395–403 (2018).
[5]B. Möller, K. Schnabel, R. Wagener, H. Kaufmann, and T. Melz, "Fatigue assessment of additively manufactured AlSi10Mg laser beam welded to rolled EN AW-6082-T6 sheet metal," Int. J. Fatigue **140**, 105805 (2020).
[6]Y. Y. Sun, P. Wang, S. L. Lu, L. Q. Li, M. L. S. Nai, and J. Wei, "Laser welding of electron beam melted Ti-6Al-4V to wrought Ti-6Al-4V: Effect of welding angle on microstructure and mechanical properties," J. Alloys Compd. **782**, 967–972 (2019).
[7]M. Nahmany, Y. Hadad, E. Aghion, A. Stern, and N. Frage, "Microstructural assessment and mechanical properties of electron beam welding of AlSi10Mg specimens fabricated by selective laser melting," J. Mater. Process. Technol. **270**, 228–240 (2019).
[8]M. Nahmany, I. Rosenthal, I. Benishti, N. Frage, and A. Stern, "Electron beam welding of AlSi10Mg workpieces produced by selected laser melting additive manufacturing technology," Addit. Manuf. **8**, 63–70 (2015).
[9]F. Scherillo, A. Astarita, U. Prisco, V. Contaldi, P. di Petta, A. Langella, and A. Squillace, "Friction stir welding of AlSi10Mg plates produced by selective laser melting," Metallogr. Microstruct. Anal. **7**, 457–463 (2018).
[10]C. Zhang, Y. Bao, H. Zhu, X. Nie, W. Zhang, S. Zhang, and X. Zeng, "A comparison between laser and TIG welding of selective laser melted AlSi10Mg," Opt. Laser Technol. **120**, 105696 (2019).
[11]C. Weingarten, D. Buchbinder, N. Pirch, W. Meiners, K. Wissenbach, and R. Poprawe, "Formation and reduction of hydrogen porosity during selective laser melting of AlSi10Mg," J. Mater. Process. Technol. **221**, 112–120 (2015).
[12]N. Chen, Z. Wan, H. P. Wang, J. Li, B. Yang, J. Solomon, and B. Carlson, "Effect of ambient pressure on laser welding of AlSi10Mg fabricated by selected laser melting," Mater. Des. **215**, 110427 (2022).
[13]C. Emmelmann and D.-I. F. Beckmann, "Optimization of laser welding process for laser additive manufactured aluminum parts by means of beam oscillation and process-oriented component design," in *Proceedings of Lasers in Manufacturing Conference* (2017).
[14]P.-O. Ulmanen, "The effect of high power adjustable ring mode fiber laser for material cutting," Master's thesis, *Tampere University of Technology* (2017)
[15]M. Mohammadpour, L. Wang, F. Kong, and R. Kovacevic, "Adjustable ring mode and single beam fiber lasers: A performance comparison," Manuf. Lett. **25**, 50–55 (2020).
[16]L. Wang, M. Mohammadpour, X. Gao, J. P. Lavoie, K. Kleine, F. Kong, and R. Kovacevic, "Adjustable ring mode (ARM) laser welding of stainless steels," Opt. Lasers Eng. **137**, 106360 (2021).
[17]M. R. Maina, Y. Okamoto, A. Okada, M. Närhi, J. Kangastupa, and J. Vihinen, "High surface quality welding of aluminum using adjustable ring-mode fiber laser," J. Mater. Process. Technol. **258**, 180–188 (2018).
[18]M. Sokolov, P. Franciosa, and D. Ceglarek, "Remote laser welding of die casting aluminum parts for automotive applications with beam oscillation and adjustable ring mode laser," in *Proceedings of Lasers in Manufacturing Conference* (2021).

[19]T. Sun, P. Franciosa, C. Liu, F. Pierro, and D. Ceglarek, "Effect of micro solidification crack on mechanical performance of remote laser welded AA6063 fillet lap joint in automotive battery tray construction," Appl. Sci. **11**, 4522 (2021).
[20]T. Sun, P. Franciosa, M. Sokolov, and D. Ceglarek, "Challenges and opportunities in laser welding of 6xxx high strength aluminium extrusions in automotive battery tray construction," Proc. CIRP **94**, 565–570 (2020).
[21]Y. Feng, X. Gao, Y. Zhang, C. Peng, X. Gui, Y. Sun, and X. Xiao, "Simulation and experiment for dynamics of laser welding keyhole and molten pool at different penetration status," Int. J. Adv. Manuf. Technol. **112**, 2301–2312 (2021).
[22]A. Mohan, D. Ceglarek, and M. Auinger, "Effect of beam oscillation on the fluid flow during laser welding," Mater. Today Proc. **59**, 1846–1851 (2022).